C-Mannosylation of *Toxoplasma gondii* proteins promotes attachment to host cells and parasite virulence

Received for publication, August 11, 2019, and in revised form, December 17, 2019 Published, Papers in Press, December 20, 2019, DOI 10.1074/jbc.RA119.010590

Andreia Albuquerque-Wendt[‡1], Damien Jacot[§], Nicolas Dos Santos Pacheco[§], Carla Seegers[‡], Patricia Zarnovican[‡], Falk F. R. Buettner[‡], Hans Bakker[‡], Dominique Soldati-Favre[§], and Françoise H. Routier[‡2]

From the [‡]Department of Clinical Biochemistry OE4340, Hannover Medical School, 30625 Hannover, Germany and the [§]Department of Microbiology and Molecular Medicine, CMU, University of Geneva, 1206 Geneva, Switzerland

Edited by Gerald W. Hart

***C*-Mannosylation is a common modification of thrombospondin type 1 repeats present in metazoans and recently identified also in apicomplexan parasites. This glycosylation is mediated by enzymes of the DPY19 family that transfer α-mannoses to tryptophan residues in the sequence WX_2WX_2C, which is part of the structurally essential tryptophan ladder. Here, deletion of the *dpy19* gene in the parasite *Toxoplasma gondii* abolished *C*-mannosyltransferase activity and reduced levels of the micronemal protein MIC2. The loss of *C*-mannosyltransferase activity was associated with weakened parasite adhesion to host cells and with reduced parasite motility, host cell invasion, and parasite egress. Interestingly, the *C*-mannosyltransferase–deficient Δ*dpy19* parasites were strongly attenuated in virulence and induced protective immunity in mice. This parasite attenuation could not simply be explained by the decreased MIC2 level and strongly suggests that absence of *C*-mannosyltransferase activity leads to an insufficient level of additional proteins. In summary, our results indicate that *T. gondii C*-mannosyltransferase DPY19 is not essential for parasite survival, but is important for adhesion, motility, and virulence.**

Toxoplasma gondii is a protozoan parasite belonging to the phylum of Apicomplexa and responsible for a worldwide spread of zoonotic infection. This obligate intracellular parasite can infect virtually all warm-blooded animals and is of high veterinary and medical importance. The disease toxoplasmosis is generally benign although the parasite establishes a chronic infection that persists in cysts throughout the hosts lifespan. In immunocompromised patients, such as HIV patients or transplant recipients, primary infection or cysts reactivation can lead to ocular toxoplasmosis, cerebral toxoplasmosis, or disseminated toxoplasmosis and can be life-threatening. When first contracted during pregnancy, congenital toxoplasmosis may lead to malformations or death of the fetus (1).

Tachyzoite, the motile and invasive form of *T. gondii*, actively and rapidly penetrates various types of cells (2, 3). Attachment of the apical pole of the parasite to host cells is followed by the formation of a moving junction formed by the apposition of the host and parasite plasma membranes, through which the parasite penetrates. A parasitophorous vacuole (PV)[3] derived from the invagination of the host cell plasma membrane is formed and sealed to provide a safe harbor and nutrient-rich milieu for parasite replication (2, 4). Parasites egress the invaded cell by rupturing both the PV and host cell plasma membranes prior to invading neighboring cells. The parasite lytic cycle relies on the sequential and regulated secretion of proteins from specialized apical organelles called micronemes and rhoptries (5, 6).

Micronemal proteins (MICs) typically contain evolutionary conserved modular domains such as epidermal growth factor-like, PAN/Apple, or thrombospondin type 1 repeats (TSRs) that mediate protein-protein and protein-carbohydrate interactions (7, 8). These interactions are involved in the formation of MIC complexes and enable attachment of the parasite to host cells (8). Several MICs (*e.g.* MIC2, MIC6, or MIC8) also interact via their cytoplasmic domain with the parasite submembrane actomyosin system and thus bridge the parasite cytoskeleton and the host cell. The actomyosin system is part of a multiprotein complex known as the glideosome that ensures translocation of MIC complexes engaged to host cell receptors from the apical pole of the parasite toward the posterior pole. This rearward translocation enables gliding motility of the parasite and is required for parasite migration through tissues, invasion of host cells, and egress from infected cells (2, 3).

Microneme exocytosis, a prerequisite to parasite attachment and gliding motility, follows a rise of the cytosolic calcium concentration. The release of calcium from the endoplasmic retic-

This work was supported by European Community Initial training network GlycoPar (EU FP7) Grant GA608295 and the European Research Council (ERC), European Union's Horizon 2020 research and innovation programme Grant 695596 (to D. S.-F.). The authors declare that they have no conflicts of interest with the contents of this article.

This article contains Fig. S1 and Tables S1–S3.

[1] This work was performed in partial fulfilment of a Ph.D. thesis carried out in the MD/Ph.D. Molecular Medicine program within the framework of the Hannover Biomedical Research School. Present address: Sir William Dunn School of Pathology, University of Oxford, South Parks Rd., OX1 3RE Oxford, United Kingdom.

[2] To whom correspondence should be addressed: Carl-Neuberg-Str. 1, 30625 Hannover, Germany. Tel.: 511-532-9807; E-mail: Routier.Francoise@mh-hannover.de.

[3] The abbreviations used are: PV, parasitophorous vacuole; MIC, micronemal protein; TSR, thrombospondin type 1 repeat; ER, endoplasmic reticulum; M2AP, MIC2-associated protein; vWF, von Willebrand factor; TRAP, thrombospondin-related anonymous protein; CSP, circumsporozoite protein; DHFR-TS, dihydrofolate reductase-thymidylate synthase; CAT, chloramphenicol acetyltransferase; ESA, excretory-secretory antigen; HFF, human foreskin fibroblast; DMEM, Dulbecco's modified Eagle's medium; sgRNA, single guide RNA; UPRT, uracil phosphoribosyltransferase; IFA, immunofluorescence assay; GA, glutaraldehyde; PFA, paraformaldehyde; ANOVA, analysis of variance.

ulum (ER) and other internal stores is typically triggered by a signaling cascade in response to a low extracellular potassium level, but can be artificially induced through ethanol exposure (6, 9, 10). After their release onto the parasite surface, MIC proteins often undergo proteolytic processing. The microneme subtilisin protease SUB1 has been shown to trim several MIC proteins such as MIC2, the MIC2-associated protein (M2AP), or MIC4, and promote efficient binding to host cell receptors (11–13). Proteolytic cleavage of the transmembrane domain of MICs shed the complex from the parasite surface and leads to the disengagement of the host-parasite interaction. To date, MIC2, MIC6, MIC8, MIC12, MIC16, and the apical membrane antigen 1 AMA1 have been shown to be cleaved by the rhomboid proteases 4 and 5 (ROM4 and ROM5) (8, 14–16).

TSRs have been described in multiple proteins and involved in various cell-cell or cell-matrix interactions (17). A repeat comprises ~60 amino acids and presents a conserved three-stranded elongated structure with six conserved cysteines that form disulfide bridges (18). In *Toxoplasma*, TSRs have been reported in the extracellular domain of the micronemal proteins MIC2, MIC12, MIC14, MIC15, MIC16, and the secreted protein with altered thrombospondin repeat domain (SPATR) (7, 8, 19–21). MIC2 has been shown to play a crucial role in parasite attachment and gliding motility, which are required for host cell invasion and parasite egress (22, 23). This type I protein contains a von Willebrand factor type A domain (vWF also known as A/I domain), six TSRs, and a short cytosolic domain. The TSRs form a semi-rigid rod-like structure that extends from the membrane and presents the vWF domain to host cell receptors such as sulfated glycoaminoglycans or intercellular adhesion molecule-1 (24–26). They bridge the vWF engaged to receptors and the cytoplasmic domain bound to the actin cytoskeleton and are thought to transmit the tensile force necessary for gliding (24). The sixth TSR of MIC2 has also been shown to associate with M2AP in the ER to form a heterohexamer (24, 27). Formation of the MIC2-M2AP complex is essential for its proper trafficking to the micronemes (22, 28, 29). In contrast to MIC2, genetic ablation of secreted protein with altered thrombospondin repeat domain did not significantly reduce adhesion or gliding motility but decreased host cell invasion (20). The function of other TSR-containing proteins remains to be established.

Two distinct types of glycosylation, α-*O*-fucosylation and α-*C*-mannosylation, have been shown to modify TSRs in metazoans and have been recently described in *Plasmodium falciparum and Plasmodium yoelii* thrombospondin-related anonymous protein (TRAP), *P. yoelli* circumsporozoite protein (CSP), and *T. gondii* MIC2 (30–35). α-*O*-Fucosylation of folded TSRs is catalyzed by the protein *O*-fucosyltransferase POFUT2 that acts on serine or threonine residues in the consensus sequence CX_{2-3}(S/T)CX_2G (which comprises conserved cysteines) (31, 32, 36–39). The β1,3-glucosyltransferase B3GLCT may then add a terminal glucose to generate the disaccharide Glcβ1–3Fucα-*O*-Ser/Thr (40–42). Protein-*O*-fucosylation occurs in the ER on folded proteins and has been shown to stabilize and promote trafficking of some TSR-containing proteins in metazoans, *P. falciparum* and *T. gondii* (31, 38, 43).

The *O*-fucosylation motif is directly preceded by a $WX_2WX_2WX_2C$ or WX_2WX_2C sequence that may carry α-mannose residues linked via a carbon–carbon bond to the tryptophan residues. The latter are part of a tryptophan-arginine ladder that plays a central role in the TSR-fold. The mannose residues are transferred from dolichol phosphate mannose by specific *C*-mannosyltransferases of the DPY19 family (44, 45). As all other glycosyltransferases that use dolichol-phosphate–activated substrate, DPY19 proteins are rather large multipass membrane glycosyltransferases localized in the ER (45). The family name originates from the dumpy phenotype observed in *Caenorhabditis elegans* worm carrying loss of function mutation in the *dpy19* gene. The phenotype associates with a defect in neuronal migration and is similar to the phenotype caused by deficiency in the *C*-mannosylated protein MIG-21 (45). In mammals, at least two DPY19 proteins (DPY19L1 and DPY19L3) are required for *C*-mannosylation of proteins having a WX_2W or WX_2C motif, including TSRs and type I cytokine receptors (44). We have recently demonstrated that *T. gondii* and *P. falciparum* DPY19 are *C*-mannosyltransferases acting on microneme proteins of the TRAP/MIC2 family (30) and investigated here the importance of *C*-mannosylation for motility, invasion, and virulence of *T. gondii* by targeted gene deletion.

Results

T. gondii protein C-mannosylation is abrogated upon dpy19 deletion

To assess the importance of *C*-mannosylation in *T. gondii*, the *dpy19* gene was replaced by a cassette encoding a pyrimethamine-resistant dihydrofolate reductase-thymidylate synthase (DHFR-TS) via homologous recombination in the RHΔ*ku80* Δ*hxgprt* strain (herein designated as WT) (Fig. 1*A*). Gene replacement was facilitated by a CRISPR/Cas9 genome editing using two guide RNAs (gRNAs) targeting the regions immediately 5′ and 3′ of *dpy19*. The resulting Δ*dpy19* strain was selected using pyrimethamine and single clones were isolated by limiting dilution. Three clones were selected and analyzed in this study. Replacement of *dpy19* was confirmed by genomic PCR analyses (Fig. 1*B*). To functionally rescue the Δ*dpy19* mutant, a plasmid encoding myc-tagged DPY19 and the selection marker chloramphenicol acetyltransferase (CAT) was transfected in the Δ*dpy19* strain. The complemented strain named Δ*dpy19*comp was selected with chloramphenicol and shown to express MycDPY19 by Western blotting (Fig. 1*C*). By immunofluorescence analysis, MycDPY19 co-localized with the transiently expressed Ty-tagged acetyl-CoA transporter AT1, previously shown to be in the ER membrane (46) (Fig. 1*D*).

To confirm the absence of functional *C*-mannosyltransferase, enzymatic assays were performed with microsomal fractions isolated from WT, Δ*dpy19*, and Δ*dpy19*comp tachyzoites (Fig. 1*E*). The microsomal preparations were incubated with radioactive GDP-Man (precursor of the dolichol-phosphate mannose donor substrate) and the acceptor peptide WAEWGEC. After incubation of the mixture, the peptide was extracted, purified by reverse phase chromatography, and the associated radioactivity was measured. The peptide WAKW,

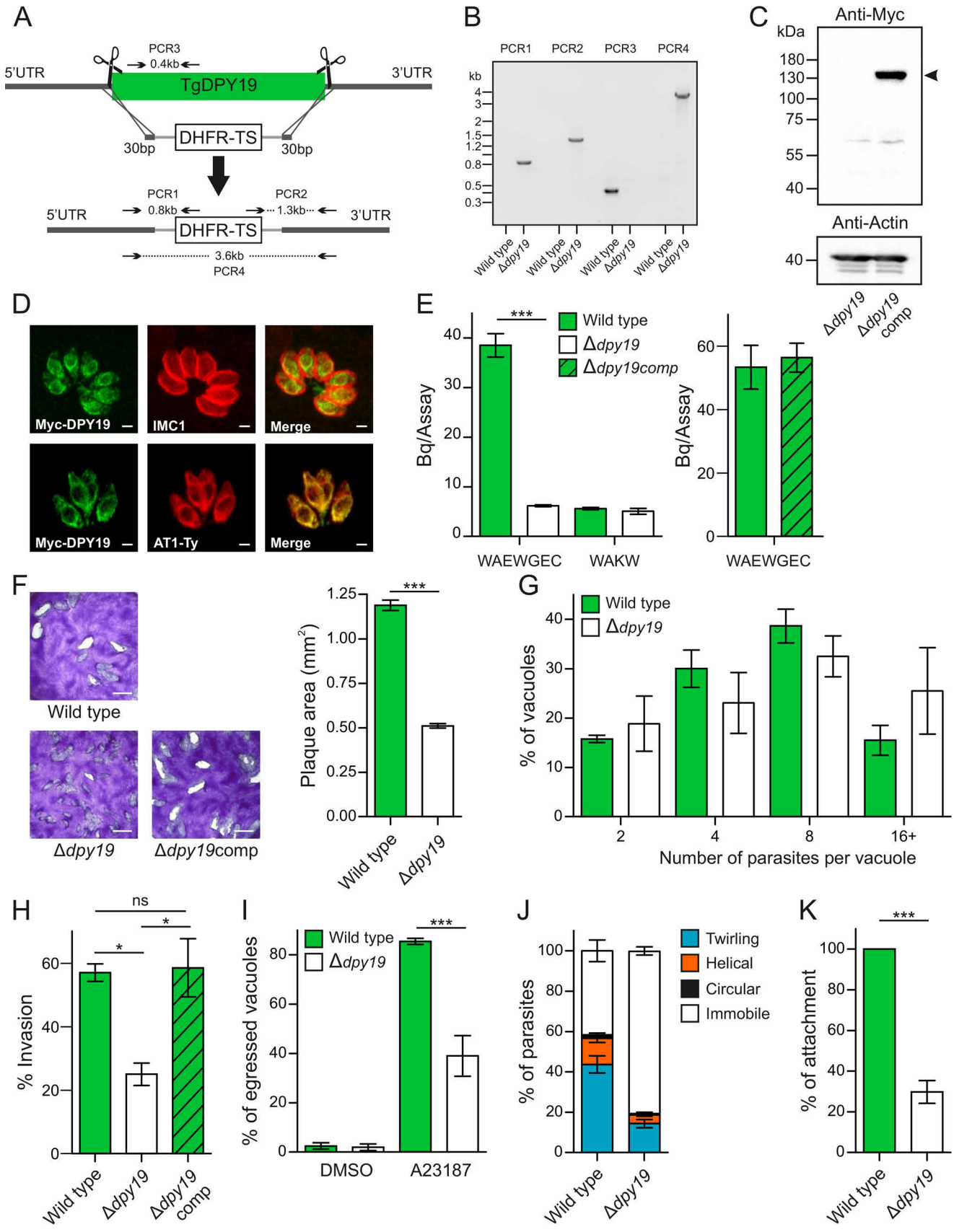
A
5'UTR
PCR3
0.4kb
TgDPY19
3'UTR
30bp
DHFR-TS
30bp
PCR1
0.8kb
PCR2
1.3kb
5'UTR
DHFR-TS
3'UTR
3.6kb
PCR4
B
PCR1
PCR2
PCR3
PCR4
kb
4
3
2
1.5
1.2
0.8
0.5
0.3
Wild type
Δdpy19
C
Anti-Myc
kDa
180
130
100
75
55
40
Anti-Actin
40
Δdpy19
Δdpy19 comp
D
Myc-DPY19
IMC1
Merge
Myc-DPY19
AT1-Ty
Merge
E
***
Wild type
Δdpy19
Δdpy19comp
Bq/Assay
WAEWGEC
WAKW
WAEWGEC
F
Wild type
Δdpy19
Δdpy19comp
***
Plaque area (mm²)
Wild type
Δdpy19
G
Wild type
Δdpy19
% of vacuoles
Number of parasites per vacuole
H
ns
*
*
% Invasion
Wild type
Δdpy19
Δdpy19 comp
I
Wild type
Δdpy19
***
% of egressed vacuoles
DMSO
A23187
J
Twirling
Helical
Circular
Immobile
% of parasites
Wild type
Δdpy19
K
***
% of attachment
Wild type
Δdpy19

which is an acceptor of mammalian DPY19 proteins but not of *T. gondii* DPY19, was used as control (30). As expected, *C*-mannosylation of the peptide WAEWGEC but not WAKW was observed in microsomes from the WT strain. Importantly, this enzymatic activity was absent in the Δ*dpy19* strain indicating that DPY19 is the only *C*-mannosyltransferase present in *T. gondii*, and was restored in the Δ*dpy19*comp strain (Fig. 1*E*).

The Δdpy19 strain presents a defect in parasite adhesion and motility

Multiple rounds of lytic cycles over 7 days of culture resulted in plaque formation within host cell monolayers. *C*-Mannosylation–deficient parasites clearly formed smaller plaques compared with the parental and Δ*dpy19*comp strains (Fig. 1*F*). A series of assays was thus carried out to define which steps of the lytic cycle were affected. We first examined the rate of replication by counting the number of parasites per vacuole, 24 h post-invasion. The Δ*dpy19* mutant did not display any defect in intracellular growth as indicated by the similar number of Δ*dpy19* or WT parasites per vacuole (Fig. 1*G*). In contrast, both the ability of Δ*dpy19* parasites to invade host cells and to egress from these cells was significantly impaired (Fig. 1, *H* and *I*). Merely 25.0% (± 6.1) of Δ*dpy19* parasites were found to invade cells as compared with 57.0% (± 4.8) for WT parasites representing a reduction of the invasion rate by ~44% (Fig. 1*H*). In contrast, invasion of cells by the Δ*dpy19*comp and WT strains was comparable (Fig. 1*H*). When infected cells were treated with the Ca^{2+} ionophore A23187 to induce parasite egress (47), 39.0% (±16.5) of Δ*dpy19* parasites containing vacuoles were able to rupture *versus* 85.5% (±2.4) for the parental strain (Fig. 1*I*).

Because host cell invasion and parasite egress are intimately connected to parasite attachment and gliding motility, we investigated these processes in Δ*dpy19* parasites and the parental strain. *In vitro* gliding assay was performed using live-video microscopy to dissect the twirling, circular, and helical movements previously described (48). Only 19.3% (±3.5) of the Δ*dpy19* parasites were motile compared with 58.3% (±9.3) of WT parasites (Fig. 1*J*). The impaired motility of Δ*dpy19* parasites was associated to a defect in attachment. Indeed, using a standard immunostaining assay, we observed that only 29.8% (± 3.7) of Δ*dpy19* parasites attached to cultured fibroblasts compared with the WT strain (Fig. 1*K*).

Loss of C-mannosylation leads to reduced MIC2 cellular level

To date, the abundant micromenal adhesin MIC2 is the only protein that has been shown to be *C*-mannosylated in *T. gondii* (30–32). In an attempt to demonstrate absence of MIC2 *C*-mannosylation in Δ*dpy19*, glycopeptides obtained by in-gel digestion with trypsin and AspN were analyzed by LC coupled to tandem MS (nanoUPLC-MS/MS). As expected, the TSR5 peptide DERPGEWAEWGECSVTCG was *C*-mannosylated and *O*-fucosylated in samples obtained from WT parasites (Fig. S1). In samples obtained from Δ*dpy19* parasites, this peptide (with or without *C*-mannosylation and/or *O*-fucosylation) was not observed, although the detection of other MIC2 peptides confirmed the presence of this protein (Fig. S1). Other peptides containing *C*-mannosylation sites were not observed. These data indirectly support absence of *C*-mannosylation in the Δ*dpy19* strain.

Given the presumed role of *C*-mannosylation in protein folding and/or stabilization (44, 45, 49, 50), we examined whether the cellular level of MIC2 was influenced by the loss of *C*-mannosylation. Lysates of WT, Δ*dpy19*, and Δ*dpy19*comp tachyzoites were analyzed by Western blotting using an anti-MIC2 antibody and an anti-tubulin antibody to normalize loading in all lanes (Fig. 2*A*). MIC2 carries at least 9 mannose residues (~1.5 kDa) (31, 32, 39), whose absence in the Δ*dpy19* strain is supported by the slightly faster migration of MIC2 when compared with the parental strain (Fig. 2*A*). Moreover, a decrease of ~50% (46 ± 15%) in MIC2 cellular level was observed in the Δ*dpy19* mutant compared with the WT (Fig. 2*A*). As expected, the migration and level of MIC2 were restored in the complemented strain Δ*dpy19*comp.

Because the level and trafficking of MIC2 was previously shown to depend on association with M2AP (22, 28), the interaction of MIC2 with M2AP was analyzed by immunoprecipitation using an anti-M2AP antibody and detection with an anti-MIC2 antibody (Fig. 2*B*). MIC2 efficiently co-immunoprecipitated with M2AP, indicating that the interaction of these two proteins was not dependent on *C*-mannosylation (Fig. 2*B*). Moreover, a decrease of the proteolytic maturation of M2AP from its proform to mature form was observed in the Δ*dpy19* mutant, which is in perfect agreement with a reduction of MIC2 cellular level (Fig. 2*B*) (22). Consistent with the formation of a complex, MIC2 and M2AP localized at the apical region of parasites, corresponding to the micronemes, in the Δ*dpy19* and WT strains (Fig. 2*C*).

Finally, to determine whether secretion and proteolytic processing of micronemal proteins was influenced by absence of *C*-mannosylation, ethanol was added to freshly egressed tachyzoites to trigger microneme secretion and the excretory-secretory antigens (ESA) were analyzed by Western blotting.

Figure 1. Deletion of *dpy19* abolishes *C*-mannosylation and leads to impaired cell invasion, parasite egress, motility, and attachment. *A,* strategy for the targeted replacement of *T. gondii dpy19* by the DHFR-TS selection cassette mediated by homologous recombination. PCRs were performed for validation of clones and the size of the expected product are indicated. *B,* validation of a Δ*dpy19* clone. Genomic DNA from the parental or Δ*dpy19* strain was used for PCR using the primer pairs AFA113/2017 (*PCR1*); 2018/AFA65 (*PCR2*); AFA01/AFA02 (*PCR3*); and AFA113/AFA65 (*PCR4*). *C,* Western blotting of Δ*dpy19 and* Δ*dpy19*comp total extracts labeled with an anti-Myc antibody confirms insertion and expression of the *dpy19* gene in the complemented mutant. *D, T. gondii* DPY19 localizes with the transiently expressed acetyl-CoA transporter AT1-Ty to the endoplasmic reticulum. *Scale bars*: 2 μm. *E, C*-mannosyltransferase activity of microsomes isolated from *T. gondii* WT, Δ*dpy19*, and Δ*dpy19*comp tachyzoites. *In vitro* assays contained GDP-[^{3}H]Man, the synthetic peptide WAEWGEC or WAKW and a microsomal fraction from WT, Δ*dpy19*, or Δ*dpy19*comp tachyzoites. *F,* representative examples and analysis of plaque areas formed in HFF monolayers inoculated with WT, Δ*dpy19*, and Δ*dpy19*comp. Fixed cells were stained with crystal violet. *Scale bars*: 2 mm. *G,* percentage of intracellular replication 24 h post-infection. The number of parasites per vacuole (2, 4, 8, 16, or more) were counted from a total of 200 vacuoles with 3 technical replicates. *H,* percentage of invasion of host cells after 30 min. *I,* percentage of ruptured vacuoles, 24 h post-infection. Egress was induced by treating the parasites with DMSO (control) or A23187. *J,* parasite motility. Gliding motility was monitored by video microscopy and 100 parasites were used to score gliding behaviors (circular, helical, or twirling) or no productive movement. *K,* percentage of parasites attached to host cells after 10 min. Mean values of three independent assays are shown for all assays ± S.D. *, *p* value <0.05; **, *p* value < 0.01; ***, *p* value <0.001 in an unpaired *t* test or one-way ANOVA.

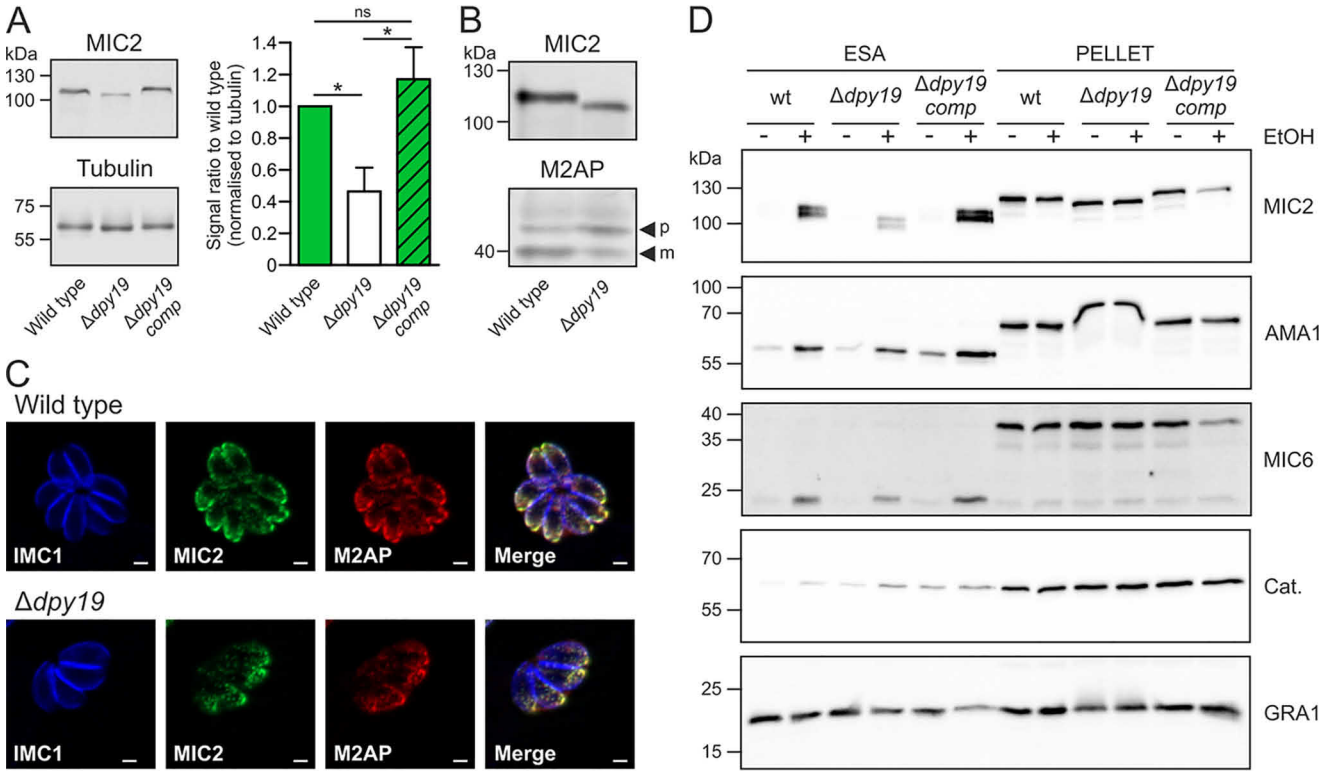

Figure 2. Absence of DPY19 leads to reduced MIC2 cellular level but does not impact on MIC2-M2AP complex formation, localization, secretion, and proteolytic processing. *A,* total extract of WT, Δ*dpy19*, and Δ*dpy19*comp parasites were analyzed by Western blotting using an anti-MIC2 antibody (*upper panel*) and an anti-tubulin antibody (*lower panel*) to normalize loading in all lanes. MIC2 levels were normalized to tubulin and the average of three biological replicates is shown. One-way ANOVA with Tukey's multiple comparison test. *, $p < 0.05$; *ns,* nonsignificant. *B,* co-immunoprecipitation of MIC2 and M2AP. M2AP was immunoprecipitated from WT and Δ*dpy19* tachyzoites lysates with rabbit anti-TgM2AP. Immunoprecipitated proteins were then analyzed by Western blotting labeled with mouse anti-TgMIC2 (*upper panel*) or rabbit anti-M2AP (*lower panel*). M2AP migrates as a proprotein (*p*) and mature protein (*m*). *C,* localization of the MIC2-M2AP complex in WT and Δ*dpy19* tachyzoites. *Scale bar*: 2 μm. *D,* secretion and proteolytic processing of the micronemal proteins MIC2, AMA1, and MIC6. WT, Δ*dpy19*, and Δ*dpy19* comp parasites were incubated in the absence (−) or presence (+) of ethanol to induce microneme secretion. The resulting pellet and ESA were then analyzed by Western blotting. Catalase (*Cat.*) was used as cytosolic control and dense granule 1 (*GRA1*) as control for constitutive secretion.

Catalase and the dense granule protein 1 (GRA1) were used as loading control for cellular and constitutively secreted proteins, respectively. Proteolytic processing and secretion of MIC6 and AMA1, which do not contain any TSR or *C*-mannosylation motif, was similar in all strains. In line with the reduced cellular level of MIC2, the relative amount of secreted MIC2, which migrated as a doublet due to differential trimming of its N terminus, was reduced in the Δ*dpy19* strain compared with the parental and complemented strain.

Deletion of dpy19 results in loss of virulence in mice and protection against a subsequent parasite challenge

To address the impact of protein *C*-mannosylation on parasite virulence, 5 mice were inoculated intraperitoneally with 50 parasites of the WT, Δ*dpy19*, or Δ*dpy19*comp strain. After 8–9 days, mice that had been infected with the WT or complemented strain were sacrificed due to severe symptoms. In contrast, mice infected with the Δ*dpy19* mutant showed no symptoms, although seroconversion confirmed infection. To determine whether these mice were protected against a subsequent challenge, 100,000 WT parasites were inoculated on day 21 after the first infection. All challenged mice survived, which indicated that Δ*dpy19* had induced protective immunity (Fig. 3).

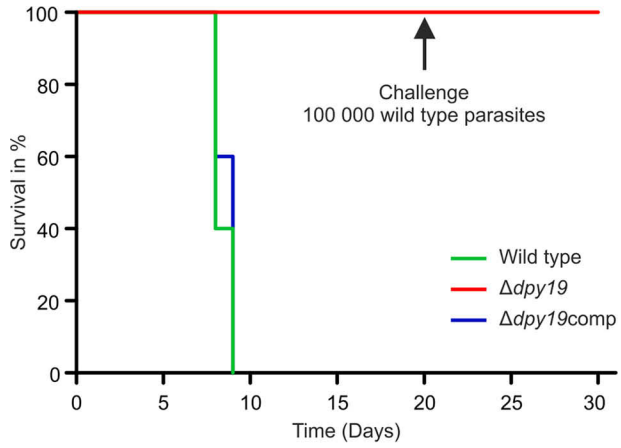

Figure 3. *T. gondii* Δ*dpy19* is strongly attenuated for virulence and confers protective immunity. Mice infected with 50 WT or Δ*dpy19*comp parasites were sacrificed after 8 to 9 days due to severe symptoms, whereas all mice infected with 50 Δ*dpy19* parasites showed no symptoms. 21 days after the first parasite injection, the surviving mice were challenged with 100,000 WT parasites and did not develop any sign of disease indicating that Δ*dpy19* confers protective immunity.

In silico prediction of C-mannosylated proteins in T. gondii

The *in vitro C*-mannosyltransferase assays presented in Fig. 1*C* confirmed that *T. gondii* DPY19 modifies the WAEWGEC peptide but, in contrast to metazoans *C*-mannosyltransferases,

does not act on the shorter WAKW peptide (Fig. 1*E*) (30, 51). These data and the few *C*-mannosylation sites described in *T. gondii, P. falciparum,* and *P. yoelii* proteins (30–35, 39) strongly suggest that apicomplexan *C*-mannosyltransferases recognize WX_2WX_2C motifs, commonly found in TSRs. A protein Blast search identified 37 *T. gondii* proteins with a WX_2WX_2C sequence. A previous study of experimentally verified *C*-mannosylation sites indicated that metazoan *C*-mannosyltransferases have a strong preference for WX_2W or WX_2C motifs with a serine, alanine, glycine, or threonine following the tryptophan residue (52). The few *C*-mannosylation sites described in apicomplexan proteins to date suggest that the parasite DPY19 enzymes have a similar specificity (30–35, 39). Tables S1 and S2 present the 14 *T. gondii* proteins containing at least one WX^*XWX^*XC motif, in which the amino acids X^* are a serine, alanine, glycine, or threonine. Besides the WX_2WX_2C motif(s), conserved cysteine, arginine, and glycine residues are present in the vast majority of these proteins and indicate their relationship to the TSR superfamily (53). These proteins represent potential substrates of *T. gondii* DPY19. This list is, however, potentially not exhaustive given that slight alterations of the WX_2WX_2C recognition motif can be tolerated, as seen by the *C*-mannosylation pattern of MIC2 (Table S2) (39), and information about the exact specificity of *C*-mannosyltransferases is still limited.

Discussion

In apicomplexans, like in metazoans, little is known about the extent and function of protein *C*-mannosylation. In this study, we analyzed the importance of this protein glycosylation for the lytic cycle and virulence of *T. gondii* tachyzoites. Deletion of the *T. gondii dpy19* gene was successful, revealing that protein *C*-mannosylation is not essential for parasite survival. Similarly, DPY19 was lately shown to be dispensable for *P. falciparum* asexual blood stages viability (54). Genetic screens predicted, however, that DPY19 confers fitness to *T. gondii* tachyzoites and *P. falciparum* asexual stages (53, 55). In agreement, DPY19 was shown to play important functions during the lytic cycle of *Toxoplasma*, as seen by the small plaques formed by the *dpy19*-deficient strain. Importantly, the plaque size was fully restored by re-expression of the *C*-mannosyltransferase. Detailed phenotyping revealed that absence of protein *C*-mannosylation severely compromised parasite adhesion, which as expected was associated with reduced motility, invasion, and egress.

The micronemal protein MIC2 secreted by tachyzoites has recently been shown to be *C*-mannosylated and *O*-fucosylated (30–32). Absence of MIC2 *C*-mannosylation in the Δ*dpy19* strain was suggested by the faster migration of MIC2 in SDS-PAGE and absence of *C*-mannosyltransferase activity in the knockout strain. Importantly, the cellular level of MIC2 was decreased by ~50% in the Δ*dpy19* strain. The formation of the MIC2-M2AP complex involves the 6th TSR of MIC2 and the modified galectin domain of M2AP (24, 27) and is determinant for the cellular level, trafficking, and secretion of both proteins (22, 28). Reduction of the MIC2 level in the Δ*dpy19* strain was, however, not due to the absence of interaction with M2AP because the two micronemal proteins co-immunoprecipitated and were co-localized at the apical pole of the parasite. In line with this result, it was recently demonstrated that the 6th TSR of MIC2 is not *C*-mannosylated and not *O*-fucosylated in *Toxoplasma* tachyzoites (24, 27, 31, 32). As expected, deletion of the *O*-fucosyltransferase POFUT2 did not affect the MIC2-M2AP complex formation either (31, 32). Together, these data confirm that association of MIC2 and its escort protein M2AP is mediated by protein-protein interaction (27).

In *T. gondii*, like in metazoan, the *C*-mannosyltransferase DPY19 localized to the ER, as is the case for other known glycosyltransferases that use dolichol-phosphate–linked donor substrate. *C*-Mannosylation might be co-translational, because folded proteins have been shown to be poor acceptor substrates *in vitro* (51). Indeed, expression of TSR-containing proteins in *C*-mannosylation– deficient cells is often associated with poor yield, suggesting that this glycosylation process assists protein folding and/or contributes to protein stability (44, 45, 49, 50, 56, 57). The involvement of *C*-mannosylation in TSR folding and stability was lately confirmed for the netrin receptor UNC5 (64). However, the requirement for *C*-mannosylation seems to vary from protein to protein. MIC2 contains 6 TSRs and is modified with at least 9 *C*-mannose residues (31, 32, 39). In the Δ*dpy19* strain, this protein might be partially misfolded and degraded by the ERAD pathway leading to the observed decrease in MIC2 level. The remaining MIC2 is presumably folded, associates with M2AP, and is properly trafficked to the micronemes before being secreted.

In the absence of MIC2, the parasite ability to attach to host cells was impaired, with severe consequences on motility and host cell invasion (22, 23). In Δ*dpy19* parasites, the observed attachment and invasion defects were less pronounced and resemble the defects reported for a mutant deficient in the protein *O*-fucosyltransferase POFUT2 (31). Note that one of the described Δ*pofut2* mutants presented significantly lower MIC2 level and an invasion defect (31), whereas the second displayed no substantial changes in attachment or MIC2 abundance (32). A third Δ*pofut2* mutant displaying a small plaque phenotype has been recently generated and might help resolve this controversy (42).

The phenotype of the Δ*dpy19* clearly differs from the phenotype of the MIC2-deficient strain Δ*mic2* because *T. gondii* preserves its virulence in the absence of MIC2 (23), whereas the lack of *C*-mannosyltransferase activity leads to a strong attenuation of virulence. A study involving simultaneous disruption of *mic1* and *mic3* has previously demonstrated that microneme proteins have synergetic roles not only in adhesion and invasion but also in virulence (58). The different virulence phenotype observed in Δ*dpy19* and Δ*mic2* strongly suggests that, in addition to MIC2, other proteins are impacted by loss of *C*-mannosyltransferase activity. Analysis of *C*-mannosylated peptides by tandem MS is the method of choice to identify *C*-mannosylated proteins. However, this method is often applied to isolated proteins and requires manual annotation of the potential glycopeptides spectra. Recently, complex protein lysates from *Plasmodium* sporozoites or *Toxoplasma* tachyzoites have been analyzed, but only the abundant surface proteins TRAP, CSP (in *P. yoelii*), and MIC2 were identified as *C*-mannosylated proteins (30–35, 39). Based on our limited knowledge of C-man-

nosyltransferases specificity, the micronemal proteins MIC12, MIC14, MIC15, and MIC16, whose functions are currently unknown, as well as several uncharacterized proteins were identified here as candidate C-mannosylated proteins. Further studies will be needed to confirm *C*-mannosylation of additional *Toxoplasma* proteins and assess their role in parasite biology and virulence.

Materials and methods

Parasite culture

T. gondii tachyzoites of RH Δ*ku80*Δ*hxgprt* strain (59), herein referred as WT or parental strain, Δ*dpy19* and Δ*dpy19*comp (this study) were maintained by serial passage on monolayers of human foreskin fibroblasts (HFF; ATCC® SCRC-1041™) cultured in Dulbecco's modified Eagle's medium (DMEM; Biochrom, Germany) supplemented with 5% (v/v) heat-inactivated fetal bovine serum (iFBS, Biochrom, Germany) at 37 °C and 5% CO_2.

Deletion of T. gondii dpy19

All primers used are listed in Table S3. A DHFR-TS selection cassette (including promoter and terminator regions) was amplified from plasmid p2854 (60) using the primers AFA96/AFA97, which each contains 30 nucleotides homologous to the 5′- or 3′-UTR of *dpy19*. Additionally, plasmid pU6-dpy19, which encodes a single guide RNA (sgRNA) targeting the region immediately upstream of the start codon (gcagactcgctctcgaaaata) and a sgRNA targeting the stop codon downstream region (agttaatcttccttctccggc) was generated and used to enhance the insertion of the DHFR-TS cassette. To generate pU6-dpy19, *T. gondii* U6 termination sequence and promoter were amplified from plasmid p2sgRNA with primers AFA102/AFA103, which each includes a sgRNA sequence. The amplicon was then cloned in the BsaI restriction site of pU6-Universal (between U6 promoter and terminator) (Addgene plasmid number 52694) (61). The resulting plasmid encodes 2 sgRNAs under *T. gondii* U6 promoter and *Streptococcus pyogenes* Cas9 under the TUB1 promoter.

Freshly egressed RH Δ*ku80*Δ*hxgprt* tachyzoites (~10^7 parasites) were pelleted at 1000 × *g* for 5 min and washed with cytomix buffer. The pellet was resuspended in cytomix buffer containing 2 mM ATP, 5 mM gluthatione, 20 μg of the plasmid pU6-dpy19, and 7 μg of the DHFR-TS selection cassette in a final volume of 800 μl. Electroporation was performed in a 4-mm cuvette with 2 pulses of 2 kV, 50 Ω, 25 microfarad. Transformants were selected using 1 μM pyrimethamine. The clonal Δ*dpy19* line was isolated by performing serial dilutions in the presence of drug selection followed by verification of integration via PCR with primer pairs AFA113/2017, 2018/AFA65, AFA113/AFA65, and AFA01/AFA02. Three clones were selected and analyzed.

Complementation of the Δdpy19 strain

For complementation of Δ*dpy19*, a plasmid coding for N terminally Myc-tagged DPY19 and the selection marker CAT was generated. Therefore, *T. gondii dpy19* coding sequence was amplified from pcDNA3.1-*dpy19* (30) using primers AFA114R and AFA115F and inserted in NsiI/PacI sites of the pTub8MycGFPPfMyoAtailTy-HXGPRT plasmid (62). The tubulin promoter and Myc-DPY19 were then amplified using AFA116F and AFA118R and inserted into the EcoRV/BglII sites of the pCAT vector, which contained 300 and 380 nucleotides homologous to the 5′- and 3′-UTR of the uracil phosphoribosyltransferase (UPRT), resulting in p5′UPRT-CAT-pTub8-mycTgDPY19–3′UPRT.

Electroporation was performed as described above with 10 μg of pSAG1Cas9gfp-U6sgUPRT plasmid (63) and 40 μg of NotI/KpnI linearized 5′-UPRT-CAT-pTub8-mycTgDPY19–3′UPRT. Parasites were selected using 20 μM chloramphenicol. The clonal Δ*dpy19*comp line was isolated by performing serial dilutions in the presence of drug selection followed by verification by Western blotting and immunofluorescence assay using a mouse hybridoma supernatant anti-Myc (1:100).

Preparation of microsomal fractions and in vitro C-mannosyltransferase assays

Approximately 10^9 tachyzoites were harvested from lysed CHO cells deficient in DPY19L1, -L2, -L3, and -L4 and suspended in 2 ml ice-cold lysis buffer (10 mM HEPES-Tris, pH 7.4, 0.8 M sorbitol, 1 mM EDTA containing protease inhibitor mixture (Roche Applied Science)) and disrupted by nitrogen cavitation at 450 p.s.i., two times, for 10 min, on ice. The homogenate was centrifuged at 1,500 × *g*, for 10 min at 4 °C. Supernatant was further centrifuged at 100,000 × *g* for 1 h and the microsomal pellets were resuspended in 200 μl of 10 mM MOPS, pH 7.5. Microsomal fractions were aliquoted and kept at −80 °C.

C-Mannosyltransferase assays were performed as previously described (30). Reactions contained microsomal fraction (10 μl representing ~35 μg of total protein), 3.7 kBq of GDP-[^{3}H]Man (American Radiolabeled Chemicals), 2 μM GDP-Man, 100 mM MOPS, pH 7.5, 0.05% saponin, 2 mM $MnCl_2$, 2 mM $MgCl_2$, 2 mM ATP, 1 mM synthetic peptide Ac-WAKW-NH_2 or Ac-WAEWGEC-NH_2 (ProteoGenix SAS) in a final volume of 25 μl and incubated for 60 min at 37 °C. Reactions were stopped by adding 230 μl of ice-cold water and 1 ml of chloroform/methanol, 3:2 (v/v). The samples were mixed, centrifuged at 3000 × *g* for 5 min, and the upper phase was diluted with 2.5 ml of 0.1% TFA (TFA) before loading onto 200-mg C18 Solid Phase Extraction Cartridges (Macherey-Nagel). The cartridges were washed 3 times with 3 ml of 0.1% TFA and peptides were eluted with 4 ml of methanol. After evaporation of the methanol, 2 ml of Luma Safe (Zinsser Analytic) were added and the samples were counted in a Beckman Coulter LS 6500.

Plaque assay

Freshly egressed parasites were inoculated on a confluent monolayer of HFF and incubated 7 days at 37 °C and 5% CO_2, after which HFF were washed once with PBS and fixed with 4% paraformaldehyde, 0.05% glutaraldehyde for 10 min. Fixed HFF were stained with crystal violet solution (0.1%) and washed three times with PBS. Plaques were measured using Fiji software version 1.8.0_66. Mean values of three independent experiments ± S.D. were determined.

Immunofluorescence assay (IFA)

Parasite-infected HFF cells seeded on coverslips were fixed in 4% paraformaldehyde (PFA), 0.05% glutaraldehyde (GA) in PBS for 10 min. After fixation, cells were rinsed once with 0.1 M glycine in PBS. Cells were permeabilized with 0.2% Triton X-100 in PBS for 20 min and blocked in PBS with 2% BSA. Cells were incubated for 60 min with primary antibodies diluted in blocking buffer, washed, and incubated for 60 min with secondary antibodies IgG Alexa Fluor 488 and 568 (1:500, Molecular Probes). Slides were viewed on a Zeiss Epifluorescence microscope using ×40 or ×63/1.4 oil objectives, imaged with an Axio Cam MRC (Zeiss) camera, and analyzed with Zen 2012 (blue edition, version 6.1.7601) software or with a Zeiss microscope (LSM700, objective apochromat 63/1.4 oil).

Intracellular growth assay

Freshly egressed parasites were allowed to invade a monolayer of HFF at 37 °C and 5% CO_2, for 24 h, after which a immunofluorescence assay was performed using mouse hybridoma supernatant anti-GRA3 (1:100) and polyclonal rabbit anti-IMC1 (1:1000) antibodies and the number of parasites per vacuole (2, 4, 8, 16, or more) were counted from a total of 200 vacuoles. Mean values of triplicates from three independent experiments ± S.D. were determined.

Invasion assay

Freshly harvested tachyzoites were added to HFF monolayer on coverslips, centrifuged at 1000 × *g* for 1 min, and allowed to invade cells for 30 min before fixation with PFA/GA. Extracellular parasites were stained using mouse hybridoma supernatant anti-SAG1 (1:100) in nonpermeabilized conditions. After three washes with PBS, cells were fixed with 1% PFA/GA for 7 min and washed once with PBS. Cells were then permeabilized with 0.2% Triton/PBS for 20 min and all parasites were stained with rabbit polyclonal anti-GAP45 (1:3000) antibody followed by IgG Alexa Fluor 488 and 568 (1:500, Molecular Probes). 200 parasites were counted and the percentage of intracellular parasites calculated. Data are mean ± S.D. from three independent biological experiments.

Induced egress assay

Freshly egressed parasites were allowed to invade a monolayer of HFF for 24 h. After which, media was exchanged for pre-warmed, serum-free DMEM containing 3 μM A23187 in DMSO and incubated for 7 min at 37 °C. IFA was performed using mouse hybridoma supernatant anti-GRA3 (1:100) and rabbit polyclonal anti-IMC1 (1:1000). For each condition, 200 vacuoles were counted and the number of lysed vacuoles was scored. Mean values of triplicates from three independent experiments ± S.D. were determined.

In vitro gliding motility assay

Gliding was monitored by video microscopy on a Nikon eclipse Ti-inverted microscope. Freshly egressed RH Δ*ku80* Δ*hxgprt* and Δ*dpy19* parasites were allowed to settle onto glass chamber slides (Ibidi) coated with 0.1% gelatin. Prior to imaging, 5-benzyl-3-isopropyl-1H-pyrazolo[4,3-d]pyrimidin-7(6H)-one (BIPPO) was added to the medium at a final concentration of 5 μM and parasites were captured by time-lapse microscopy for 1 min in several areas of the chamber using a ×63 Oil Plan Apochromat objective. One hundred parasites were used to score gliding behaviors (*i.e.* circular, helical, or twirling) or no productive movement. Experiments have been done in triplicate.

Attachment assay

Attachment assay was conducted as described previously (23). Briefly, 10^6 freshly egressed tachyzoites were inoculated on a confluent monolayer of HFF and incubated for 10 min at 37 °C and 5% CO_2, after which cells were washed once with PBS. IFA was performed using mouse hybridoma supernatant anti-SAG1 (1:100) and total numbers of parasites within 15 fields of view (objective ×60) were counted. Mean value of triplicates from three independent experiments ± S.D. were determined.

Cellular localization of DPY19

T. gondii at1 (TgME49_215940) was amplified from cDNA using primers DSF5272/DSF5273 and inserted in EcoRI/NsiI sites of pTub8MycGFPPfMyoAtailTy-XGPRT plasmid (62) to generate the pTub8-AT1Ty-HXGPRT plasmid. Around 10 μg of the plasmid were then transiently transfected in the Δ*dpy19*comp strain. Immunofluorescence assay using anti-Myc (DPY19) and anti-Ty (AT1) antibodies was performed the next day.

Mass spectrometry analyses

WT and Δ*dpy19* tachyzoites were disrupted in 500 mM Tris-HCl, pH 8.5, 50 mM EDTA, 700 mM sucrose, 100 mM KCl, 1% SDS, and 2% β-mercaptoethanol by sonification 8 × 30 s on ice (~10^8 parasites/ml). One volume of Roti-phenol, pH 7.5–8.0 (Roth), was added to samples and mixed by inversion for 10 min at 4 °C. The phenol phase was precipitated with 4 volumes of 0.1 M ammonium acetate in cold methanol at −20 °C for at least 4 h. The pellet recovered by centrifugation at 6000 × *g* for 10 min at 4 °C was solubilized in Laemmli buffer and proteins (equivalent to 5 × 10^7 parasites/lane) were separated on a 10% SDS-PAGE gel. The MIC2-containing bands were manually excised from Coomassie gel and treated as previously described (30). Briefly the proteins were reduced with 10 mM DTT, alkylated with 100 mM iodoacetamide, and digested at 37 °C with 0.1 μM trypsin followed by digestion with 0.1 μg of AspN (Promega). The resulting peptides were extracted from gel pieces with 50% acetonitrile containing 5% formic acid, followed by 75% acetonitrile containing 0.5% formic acid, and finally 100% acetonitrile. Extracts were dried and dissolved in 2% acetonitrile containing 0.1% TFA. A Waters nanoACQUITY-UPLC System equipped with an analytical column (Waters, BEH130 C18, 100 × 100 μm, 1.7-μm particle size) coupled online to an ESI-Q-TOF Ultima was used for analysis as previously described (44). Obtained spectra were explored with MassLynx version 4.1 software (Waters). The theoretical mass of each peptide containing putative *C*-mannosylation sites was calculated with or without glycosylation (*C*-mannosylation and

O-fucosylation). Extracted ion chromatograms were generated by ion counts for these masses (±0.1Da).

Analysis of MIC2 cellular level by Western blotting

Tachyzoites were harvested, centrifuged at 1500 × *g* for 10 min, suspended at a concentration of 10^8 parasites/ml in Laemmli buffer, and disrupted by sonification 8 × 30 s on ice. 1% β-Mercaptoethanol was added and samples were heated at 95 °C for 10 min. Protein were separated by SDS-PAGE on a 12% acrylamide gel and blotted onto nitrocellulose membrane. The membrane was stained with mouse anti-MIC2 6D10 hybridoma supernatant (1:100) or mouse anti-α-tubulin (1:800) (Developmental Studies Hybridoma Bank) followed by an anti-mouse IRdye800CW (1:20,000) (LiCor Biosciences) in Odyssey buffer (LiCor Biosciences). Labeled membranes were detected using LiCor Odyssey IR imager 1060 version 2.1.12, and the images processed with Image Studio version 4.0.21.

MIC2-M2AP co-immunoprecipitation

HFF monolayers from a 6-cm^2 dish were infected with tachyzoites. 48 h post-infection, extracellular and intracellular parasites were purified by passaging the cell-parasite suspension two times through 27-gauge needles (Braun), washed once with PBS, pelleted, and resuspended in 0.5 ml of immunoprecipitation buffer (1% Triton X-100, 50 mM Tris-HCl, pH 8.0, 150 mM NaCl, EDTA-free proteases inhibitor (Roche Applied Science). Parasite suspension was freeze-thawed five times, sonicated 3 × 10 s on ice, and centrifuged 14,000 × *g* for 30 min at 4 °C. Supernatant was incubated with a rabbit anti-M2AP antibody for 60 min at 4 °C on a rotating wheel. After incubation, 0.1 ml of Protein A-Sepharose™ CL-4B (GE Healthcare Life Sciences) beads was added to the suspension and the sample was incubated for 1 h at 4 °C on a rotating wheel. Complexes were washed 4 times in 1 ml of immunoprecipitation buffer with intermediate centrifugation at 1,500 × *g* for 1 min, at 4 °C. The remaining pellet was suspended in protein loading buffer with 5% DTT, separated in a 12% SDS-polyacrylamide gels, and transferred to a nitrocellulose membrane. Western blots were processed using anti-MIC2 antibody for 60 min, washed, and incubated with IRDye LiCor secondary antibody for another 60 min. Labeled membranes were detected using Li-Cor Odyssey IR imager ODY 1060 version 2.1.12, and the images processed with Image Studio version 4.0.21.

Microneme secretion assay

Freshly egressed parasites were harvested, washed twice with pre-warmed intracellular buffer (5 mM NaCl, 142 mM KCl, 1 mM $MgCl_2$, 2 mM EGTA, 5.6 mM glucose, and 25 mM HEPES, pH 7.2), equally distributed in two Eppendorf tubes, and resuspended in previously warmed DMEM with 5% FCS and ±2% EtOH. Parasite suspension was incubated at 37 °C for 30 min, followed by centrifugation at 1000 × *g*, 4 °C, for 5 min. Supernatants (with constitutively or induced secreted micronemal proteins) were collected and centrifuged at 2000 × *g*, 4 °C, for an additional 5 min to remove residual parasite debris. Pellets were washed once in PBS. ESA and pellets were separated in a 12% SDS-polyacrylamide gels and transferred to a nitrocellulose membrane. Membranes were blocked in 3% BSA, 0.02% Tween in PBS (PBST) for 30 min. Western blots were processed using a combination of primary antibodies for 60 min, washed, and incubated with secondary antibodies an additional 60 min. Labeled membranes were detected using GE Healthcare-Amersham Biosciences ECL Western Blotting Detection Reagent and visualized on a Bio-Rad ChemiDoc™ MP Imaging system or directly visualized on a Li-Cor Odyssey IR imager ODY 1060 version 2.1.12, and the images processed with Image Studio version 4.0.21.

Mouse infection

For each strain (WT, Δ*dpy19*, and Δ*dpy19*comp), 5 CD1 mice (female, 6 weeks, Charles River Laboratories) were infected with 50 parasites by intraperitoneal injection (day 1). The health of the mice was monitored daily until they presented severe symptoms of acute toxoplasmosis (bristled hair and complete prostration with incapacity to drink or eat) and were sacrificed on that day. Because they showed no symptoms, the 5 mice infected with Δ*dpy19* parasites were challenged with 10^5 WT parasites at day 21.

Ethics statement

The animal experiments were conducted with the authorization number 1026/3604/2, GE30/l3 according to the guidelines and regulations issues by the Swiss Federal Veterinary Office. No human samples were used in these experiments.

Author contributions—A. A.-W., D. J., N. D. S. P., H. B., D. S.-F., and F. H. R. conceptualization; A. A.-W., D. J., N. D. S. P., D. S.-F., and F. H. R. formal analysis; A. A.-W., D. J., N. D. S. P., C. S., P. Z., H. B., and F. H. R. validation; A. A.-W., D. J., N. D. S. P., C. S., P. Z., F. F. R. B., H. B., and F. H. R. investigation; A. A.-W., D. J., N. D. S. P., C. S., P. Z., H. B., and F. H. R. visualization; A. A.-W., D. J., N. D. S. P., C. S., P. Z., H. B., and F. H. R. methodology; A. A.-W. and F. H. R. writing-original draft; A. A.-W., D. J., N. D. S. P., H. B., D. S.-F., and F. H.R. writing-review and editing; D. J., H. B., and F. H. R. supervision; D. S.-F. and F. H. R. funding acquisition; D. S.-F. and F. H. R. project administration.

Acknowledgments—We thank Dr. Rebecca Oppenheim for the generation of the pTub8-AT1Ty-HXGPRT vector. We thank Dr. John Crawford Samuelson and Dr. Giulia Bandini for helpful discussions and Dr. Mae Huynh and Dr. Vern Carruthers for the kind gift of antibodies and technical advices.

References

1. Robert-Gangneux, F., and Dardé, M. L. (2012) Epidemiology of and diagnostic strategies for toxoplasmosis. *Clin. Microbiol. Rev.* **25,** 264–296 CrossRef Medline
2. Frénal, K., Dubremetz, J. F., Lebrun, M., and Soldati-Favre, D. (2017) Gliding motility powers invasion and egress in apicomplexa. *Nat. Rev. Microbiol.* **15,** 645–660 CrossRef Medline
3. Bargieri, D., Lagal, V., Andenmatten, N., Tardieux, I., Meissner, M., and Ménard, R. (2014) Host cell invasion by apicomplexan parasites: the junction conundrum. *PLoS Pathog.* **10,** e1004273 CrossRef Medline
4. Coppens, I., and Romano, J. D. (2018) Hostile intruder: *Toxoplasma* holds host organelles captive. *PLoS Pathog.* **14,** e1006893 CrossRef Medline
5. Carruthers, V. B., and Sibley, L. D. (1997) Sequential protein secretion from three distinct organelles of *Toxoplasma gondii* accompanies invasion of human fibroblasts. *Eur. J. Cell Biol.* **73,** 114–123 Medline

6. Dubois, D. J., and Soldati-Favre, D. (2019) Biogenesis and secretion of micronemes in *Toxoplasma gondii*. *Cell. Microbiol.* **21,** e13018 CrossRef Medline
7. Sheiner, L., Santos, J. M., Klages, N., Parussini, F., Jemmely, N., Friedrich, N., Ward, G. E., and Soldati-Favre, D. (2010) *Toxoplasma gondii* transmembrane microneme proteins and their modular design. *Mol. Microbial.* **77,** 912–929 Medline
8. Liu, Q., Li, F. C., Zhou, C. X., and Zhu, X. Q. (2017) Research advances in interactions related to *Toxoplasma gondii* microneme proteins. *Exp. Parasitol.* **176,** 89–98 CrossRef Medline
9. Carruthers, V. B., Moreno, S. N., and Sibley, L. D. (1999) Ethanol and acetaldehyde elevate intracellular [Ca^{2+}] and stimulate microneme discharge in *Toxoplasma gondii*. *Biochem. J.* **342**, 379–386 Medline
10. Carruthers, V. B., and Sibley, L. D. (1999) Mobilization of intracellular calcium stimulates microneme discharge in *Toxoplasma gondii*. *Mol. Microbiol.* **31,** 421–428 CrossRef Medline
11. Lagal, V., Binder, E. M., Huynh, M. H., Kafsack, B. F., Harris, P. K., Diez, R., Chen, D., Cole, R. N., Carruthers, V. B., and Kim, K. (2010) *Toxoplasma gondii* protease TgSUB1 is required for cell surface processing of microneme adhesive complexes and efficient adhesion of tachyzoites. *Cell. Microbiol.* **12,** 1792–1808 CrossRef Medline
12. Saouros, S., Dou, Z., Henry, M., Marchant, J., Carruthers, V. B., and Matthews, S. (2012) Microneme protein 5 regulates the activity of *Toxoplasma* subtilisin 1 by mimicking a subtilisin prodomain. *J. Biol. Chem.* **287,** 36029–36040 CrossRef Medline
13. Carruthers, V. B., Sherman, G. D., and Sibley, L. D. (2000) The Toxoplasma adhesive protein MIC2 is proteolytically processed at multiple sites by two parasite-derived proteases. *J. Biol. Chem.* **275,** 14346–14353 CrossRef Medline
14. Buguliskis, J. S., Brossier, F., Shuman, J., and Sibley, L. D. (2010) Rhomboid 4 (ROM4) affects the processing of surface adhesins and facilitates host cell invasion by *Toxoplasma gondii*. *PLoS Pathog.* **6,** e1000858 CrossRef Medline
15. Rugarabamu, G., Marq, J. B., Guérin, A., Lebrun, M., and Soldati-Favre, D. (2015) Distinct contribution of *Toxoplasma gondii* rhomboid proteases 4 and 5 to micronemal protein protease 1 activity during invasion. *Mol. Microbiol.* **97,** 244–262 CrossRef Medline
16. Shen, B., Buguliskis, J. S., Lee, T. D., and Sibley, L. D. (2014) Functional analysis of rhomboid proteases during *Toxoplasma* invasion. *mBio* **5,** e01795-14 Medline
17. Adams, J. C., and Tucker, R. P. (2000) The thrombospondin type 1 repeat (TSR) superfamily: diverse proteins with related roles in neuronal development. *Dev. Dyn.* **218,** 280–299 CrossRef
18. Tan, K., Duquette, M., Liu, J. H., Dong, Y., Zhang, R., Joachimiak, A., Lawler, J., and Wang, J. H. (2002) Crystal structure of the TSP-1 type 1 repeats: a novel layered fold and its biological implication. *J. Cell Biol.* **159,** 373–382 CrossRef Medline
19. Kawase, O., Nishikawa, Y., Bannai, H., Igarashi, M., Matsuo, T., and Xuan, X. (2010) Characterization of a novel thrombospondin-related protein in *Toxoplasma gondii*. *Parasitol. Int.* **59,** 211–216 CrossRef Medline
20. Huynh, M. H., Boulanger, M. J., and Carruthers, V. B. (2014) A conserved apicomplexan microneme protein contributes to *Toxoplasma gondii* invasion and virulence. *Infect. Immun.* **82,** 4358–4368 CrossRef Medline
21. Lebrun, M., Caruthers, V. B., and Cesbron-Delauw, M.-F. (2013) *Toxoplasma Secretory Proteins and Their Roles in Cell Invasion and Intracellular Survival*, Academic Press, New York
22. Huynh, M. H., and Carruthers, V. B. (2006) Toxoplasma MIC2 is a major determinant of invasion and virulence. *PLoS Pathog.* **2,** e84 CrossRef Medline
23. Gras, S., Jackson, A., Woods, S., Pall, G., Whitelaw, J., Leung, J. M., Ward, G. E., Roberts, C. W., and Meissner, M. (2017) Parasites lacking the micronemal protein MIC2 are deficient in surface attachment and host cell egress, but remain virulent *in vivo*. *Wellcome Open Res.* **2,** 32 CrossRef Medline
24. Song, G., and Springer, T. A. (2014) Structures of the *Toxoplasma* gliding motility adhesin. *Proc. Natl. Acad. Sci. U.S.A.* **111,** 4862–4867 CrossRef Medline
25. Harper, J. M., Hoff, E. F., and Carruthers, V. B. (2004) Multimerization of the *Toxoplasma gondii* MIC2 integrin-like A-domain is required for binding to heparin and human cells. *Mol. Biochem. Parasitol.* **134,** 201–212 CrossRef Medline
26. Barragan, A., Brossier, F., and Sibley, L. D. (2005) Transepithelial migration of *Toxoplasma gondii* involves an interaction of intercellular adhesion molecule 1 (ICAM-1) with the parasite adhesin MIC2. *Cell. Microbiol.* **7,** 561–568 CrossRef Medline
27. Huynh, M. H., Liu, B., Henry, M., Liew, L., Matthews, S. J., and Carruthers, V. B. (2015) Structural basis of *Toxoplasma gondii* MIC2-associated protein interaction with MIC2. *J. Biol. Chem.* **290,** 1432–1441 CrossRef Medline
28. Huynh, M. H., Rabenau, K. E., Harper, J. M., Beatty, W. L., Sibley, L. D., and Carruthers, V. B. (2003) Rapid invasion of host cells by *Toxoplasma* requires secretion of the MIC2-M2AP adhesive protein complex. *EMBO J.* **22,** 2082–2090 CrossRef Medline
29. Harper, J. M., Huynh, M. H., Coppens, I., Parussini, F., Moreno, S., and Carruthers, V. B. (2006) A cleavable propeptide influences *Toxoplasma* infection by facilitating the trafficking and secretion of the TgMIC2-M2AP invasion complex. *Mol. Biol. Cell* **17,** 4551–4563 CrossRef Medline
30. Hoppe, C. M., Albuquerque-Wendt, A., Bandini, G., Leon, D. R., Shcherbakova, A., Buettner, F. F. R., Izquierdo, L., Costello, C. E., Bakker, H., and Routier, F. H. (2018) Apicomplexan C-mannosyltransferases modify thrombospondin type I-containing adhesins of the TRAP family. *Glycobiology* **28,** 333–343 CrossRef Medline
31. Bandini, G., Leon, D. R., Hoppe, C. M., Zhang, Y., Agop-Nersesian, C., Shears, M. J., Mahal, L. K., Routier, F. H., Costello, C. E., and Samuelson, J. (2019) *O*-Fucosylation of thrombospondin-like repeats is required for processing of microneme protein 2 and for efficient host cell invasion by *Toxoplasma gondii* tachyzoites. *J. Biol. Chem.* **294,** 1967–1983 CrossRef Medline
32. Khurana, S., Coffey, M. J., John, A., Uboldi, A. D., Huynh, M. H., Stewart, R. J., Carruthers, V. B., Tonkin, C. J., Goddard-Borger, E. D., and Scott, N. E. (2019) Protein *O*-fucosyltransferase 2-mediated *O*-glycosylation of the adhesin MIC2 is dispensable for *Toxoplasma gondii* tachyzoite infection. *J. Biol. Chem.* **294,** 1541–1553 CrossRef Medline
33. Swearingen, K. E., Lindner, S. E., Shi, L., Shears, M. J., Harupa, A., Hopp, C. S., Vaughan, A. M., Springer, T. A., Moritz, R. L., Kappe, S. H., and Sinnis, P. (2016) Interrogating the plasmodium sporozoite surface: identification of surface-exposed proteins and demonstration of glycosylation on CSP and TRAP by mass spectrometry-based proteomics. *PLoS Pathog.* **12,** e1005606 CrossRef Medline
34. Swearingen, K. E., Lindner, S. E., Flannery, E. L., Vaughan, A. M., Morrison, R. D., Patrapuvich, R., Koepfli, C., Muller, I., Jex, A., Moritz, R. L., Kappe, S. H. I., Sattabongkot, J., and Mikolajczak, S. A. (2017) Proteogenomic analysis of the total and surface-exposed proteomes of *Plasmodium vivax* salivary gland sporozoites. *PLoS Negl. Trop. Dis.* **11,** e0005791 CrossRef Medline
35. Swearingen, K. E., Eng, J. K., Shteynberg, D., Vigdorovich, V., Springer, T. A., Mendoza, L., Sather, D. N., Deutsch, E. W., Kappe, S. H. I., and Moritz, R. L. (2019) A tandem mass spectrometry sequence database search method for identification of *O*-fucosylated proteins by mass spectrometry. *J. Proteome Res.* **18,** 652–663 CrossRef Medline
36. Luo, Y., Nita-Lazar, A., and Haltiwanger, R. S. (2006) Two distinct pathways for *O*-fucosylation of epidermal growth factor-like or thrombospondin type 1 repeats. *J. Biol. Chem.* **281,** 9385–9392 CrossRef Medline
37. Luo, Y., Koles, K., Vorndam, W., Haltiwanger, R. S., and Panin, V. M. (2006) Protein *O*-fucosyltransferase 2 adds *O*-fucose to thrombospondin type 1 repeats. *J. Biol. Chem.* **281,** 9393–9399 CrossRef Medline
38. Lopaticki, S., Yang, A. S. P., John, A., Scott, N. E., Lingford, J. P., O'Neill, M. T., Erickson, S. M., McKenzie, N. C., Jennison, C., Whitehead, L. W., Douglas, D. N., Kneteman, N. M., Goddard-Borger, E. D., and Boddey, J. A. (2017) Protein *O*-fucosylation in *Plasmodium falciparum* ensures efficient infection of mosquito and vertebrate hosts. *Nat. Commun.* **8,** 561 CrossRef Medline
39. Bandini, G., Albuquerque-Wendt, A., Hegermann, J., Samuelson, J., and Routier, F. H. (2019) Protein *O*- and *C*-glycosylation pathways in *Toxo-*

plasma gondii and *Plasmodium falciparum*. *Parasitology* **146,** 1755–1766 CrossRef Medline
40. Kozma, K., Keusch, J. J., Hegemann, B., Luther, K. B., Klein, D., Hess, D., Haltiwanger, R. S., and Hofsteenge, J. (2006) Identification and characterization of abeta1,3-glucosyltransferase that synthesizes the Glc-β1,3-Fuc disaccharide on thrombospondin type 1 repeats. *J. Biol. Chem.* **281,** 36742–36751 CrossRef Medline
41. Sato, T., Sato, M., Kiyohara, K., Sogabe, M., Shikanai, T., Kikuchi, N., Togayachi, A., Ishida, H., Ito, H., Kameyama, A., Gotoh, M., and Narimatsu, H. (2006) Molecular cloning and characterization of a novel human β1,3-glucosyltransferase, which is localized at the endoplasmic reticulum and glucosylates *O*-linked fucosylglycan on thrombospondin type 1 repeat domain. *Glycobiology* **16,** 1194–1206 CrossRef Medline
42. Gas-Pascual, E., Ichikawa, H. T., Sheikh, M. O., Serji, M. I., Deng, B., Mandalasi, M., Bandini, G., Samuelson, J., Wells, L., and West, C. M. (2019) CRISPR/Cas9 and glycomics tools for *Toxoplasma* glycobiology. *J. Biol. Chem.* **294,** 1104–1125 CrossRef Medline
43. Vasudevan, D., and Haltiwanger, R. S. (2014) Novel roles for *O*-linked glycans in protein folding. *Glycoconj. J.* **31,** 417–426 CrossRef Medline
44. Shcherbakova, A., Tiemann, B., Buettner, F. F., and Bakker, H. (2017) Distinct C-mannosylation of netrin receptor thrombospondin type 1 repeats by mammalian DPY19L1 and DPY19L3. *Proc. Natl. Acad. Sci. U.S.A.* **114,** 2574–2579 CrossRef Medline
45. Buettner, F. F., Ashikov, A., Tiemann, B., Lehle, L., and Bakker, H. (2013) *C. elegans* DPY-19 is a *C*-mannosyltransferase glycosylating thrombospondin repeats. *Mol. Cell* **50,** 295–302 CrossRef Medline
46. Tymoshenko, S., Oppenheim, R. D., Agren, R., Nielsen, J., Soldati-Favre, D., and Hatzimanikatis, V. (2015) Metabolic needs and capabilities of *Toxoplasma gondii* through combined computational and experimental analysis. *PLoS Comp. Biol.* **11,** e1004261 CrossRef Medline
47. Moudy, R., Manning, T. J., and Beckers, C. J. (2001) The loss of cytoplasmic potassium upon host cell breakdown triggers egress of *Toxoplasma gondii*. *J. Biol. Chem.* **276,** 41492–41501 CrossRef Medline
48. Håkansson, S., Morisaki, H., Heuser, J., and Sibley, L. D. (1999) Time-lapse video microscopy of gliding motility in *Toxoplasma gondii* reveals a novel, biphasic mechanism of cell locomotion. *Mol. Biol. Cell* **10,** 3539–3547 CrossRef Medline
49. Siupka, P., Hamming, O. T., Kang, L., Gad, H. H., and Hartmann, R. (2015) A conserved sugar bridge connected to the WSXWS motif has an important role for transport of IL-21R to the plasma membrane. *Genes Immun.* **16,** 405–413 CrossRef Medline
50. Niwa, Y., Suzuki, T., Dohmae, N., and Simizu, S. (2016) Identification of DPY19L3 as the *C*-mannosyltransferase of R-spondin1 in human cells. *Mol. Biol. Cell* **27,** 744–756 CrossRef Medline
51. Doucey, M. A., Hess, D., Cacan, R., and Hofsteenge, J. (1998) Protein C-mannosylation is enzyme-catalysed and uses dolichyl-phosphate-mannose as a precursor. *Mol. Biol. Cell* **9,** 291–300 CrossRef Medline
52. Julenius, K. (2007) NetCGlyc 1.0: prediction of mammalian *C*-mannosylation sites. *Glycobiology* **17,** 868–876 CrossRef Medline
53. Sidik, S. M., Huet, D., Ganesan, S. M., Huynh, M. H., Wang, T., Nasamu, A. S., Thiru, P., Saeij, J. P. J., Carruthers, V. B., Niles, J. C., and Lourido, S. (2016) A genome-wide CRISPR screen in *Toxoplasma* identifies essential apicomplexan genes. *Cell* **166,** 1423–1435.e12 CrossRef Medline
54. Lopez-Gutierrez, B., Cova, M., and Izquierdo, L. (2019) A *Plasmodium falciparum C*-mannosyltransferase is dispensable for parasite asexual blood stage development. *Parasitology* **146,** 1767–1772 CrossRef Medline
55. Zhang, M., Wang, C., Otto, T. D., Oberstaller, J., Liao, X., Adapa, S. R., Udenze, K., Bronner, I. F., Casandra, D., Mayho, M., Brown, J., Li, S., Swanson, J., Rayner, J. C., Jiang, R. H. Y., and Adams, J. H. (2018) Uncovering the essential genes of the human malaria parasite *Plasmodium falciparum* by saturation mutagenesis. *Science* **360,** eaap7847 CrossRef Medline
56. Munte, C. E., Gäde, G., Domogalla, B., Kremer, W., Kellner, R., and Kalbitzer, H. R. (2008) *C*-Mannosylation in the hypertrehalosaemic hormone from the stick insect *Carausius morosus*. *FEBS J.* **275,** 1163–1173 CrossRef Medline
57. Wang, L. W., Leonhard-Melief, C., Haltiwanger, R. S., and Apte, S. S. (2009) Post-translational modification of thrombospondin type-1 repeats in ADAMTS-like 1/punctin-1 by *C*-mannosylation of tryptophan. *J. Biol. Chem.* **284,** 30004–30015 CrossRef Medline
58. Cérède, O., Dubremetz, J. F., Bout, D., and Lebrun, M. (2002) The *Toxoplasma gondii* protein MIC3 requires pro-peptide cleavage and dimerization to function as adhesin. *EMBO J.* **21,** 2526–2536 CrossRef Medline
59. Fox, B. A., Ristuccia, J. G., Gigley, J. P., and Bzik, D. J. (2009) Efficient gene replacements in *Toxoplasma gondii* strains deficient for nonhomologous end joining. *Eukaryot. Cell* **8,** 520–529 CrossRef Medline
60. Donald, R. G., and Roos, D. S. (1993) Stable molecular transformation of *Toxoplasma gondii*: a selectable dihydrofolate reductase-thymidylate synthase marker based on drug-resistance mutations in malaria. *Proc. Natl. Acad. Sci. U.S.A.* **90,** 11703–11707 CrossRef Medline
61. Sidik, S. M., Hackett, C. G., Tran, F., Westwood, N. J., and Lourido, S. (2014) Efficient genome engineering of *Toxoplasma gondii* using CRISPR/Cas9. *PloS One* **9,** e100450 CrossRef Medline
62. Hettmann, C., Herm, A., Geiter, A., Frank, B., Schwarz, E., Soldati, T., and Soldati, D. (2000) A dibasic motif in the tail of a class XIV apicomplexan myosin is an essential determinant of plasma membrane localization. *Mol. Biol. Cell* **11,** 1385–1400 CrossRef Medline
63. Shen, B., Brown, K., Long, S., and Sibley, L. D. (2017) Development of CRISPR/Cas9 for efficient genome editing in *Toxoplasma gondii*. *Methods Mol. Biol. (Clifton, N.J.)* **1498,** 79–103 CrossRef Medline
64. Shcherbakova, A., Preller, M., Taft, M. H., Pujols, J., Ventura, S., Tiemann, B., Buettner, F. F. R., and Bakker, H. (2019) C-Mannosylation supports folding and enhances stability of thrombospondin repeats. *Elife* **8,** pii: e529788 CrossRef Medline